Science Advances
AAAS

advances.sciencemag.org/cgi/content/full/7/9/eabb7403/DC1

Supplementary Materials for

Strong local, not global, controls on marine pyrite sulfur isotopes

V. Pasquier*, R. N. Bryant, D. A. Fike, I. Halevy

*Corresponding author. Email: virgil.pasquier@weizmann.ac.il

Published 26 February 2021, *Sci. Adv.* **7**, eabb7403 (2021)
DOI: 10.1126/sciadv.abb7403

This PDF file includes:

Supplementary Text

$\delta^{34}S_{pyr}$ and sea level dependence

Over the first 500 m of IODP borehole 1352 (i.e., shelf location), $\delta^{34}S_{pyr}$ values are low and relatively invariant in the sandstone layers, whereas mud(stone)/marlstone layers are characterized by higher $\delta^{34}S_{pyr}$ values and variability. We also note that in most of the cases, the highest $\delta^{34}S_{pyr}$ values are observed at the contact between the sandy and muddy units. To explore this lithological dependence, we used the high-resolution foraminifera $\delta^{18}O$ record available over the first 500 m. We found that the muddy layers were rapidly accumulated over (glacial) periods of sea-level regression, as a result of decreasing accommodation space on the shelf. River mouths (the Waiau River and other coastal rivers) advanced towards the shelf edge, supplying clay to the upper slope, and increasing the sedimentation rate at the study site by a factor of ~6 (average value) relative to interglacial periods. Consequently, the diagenetic system became more burial-dominated, where MSR exhausts the porewater sulfate reservoir, leading to a progressive ^{34}S enrichment of the residual sulfate (and product sulfide) with depth in the sediments due to Rayleigh distillation.

Rapid elevation of sea level due to ice-sheet melting during the termination of ice ages inundated the shelf, generating ample space to accommodate the pro-deltaic deposits. The coastline and associated terrigenous deposits migrated landward, initiating the deposition of transgressive units until maximum flooding occurred. At times of maximum sea level, fine-grained terrigenous sediment no longer reached the upper slope, and sediment accumulation was maintained by smaller fluxes of pelagic skeletal material, as supported by downcore variation in Ca/Sr and Ca/Ti ratios, leading to the deposition of sandy-mud layers. As a result, during interglacial intervals, sedimentation rates were lower than 0.2 m/kyr, resulting in good communication between the porewater and the overlying seawater.

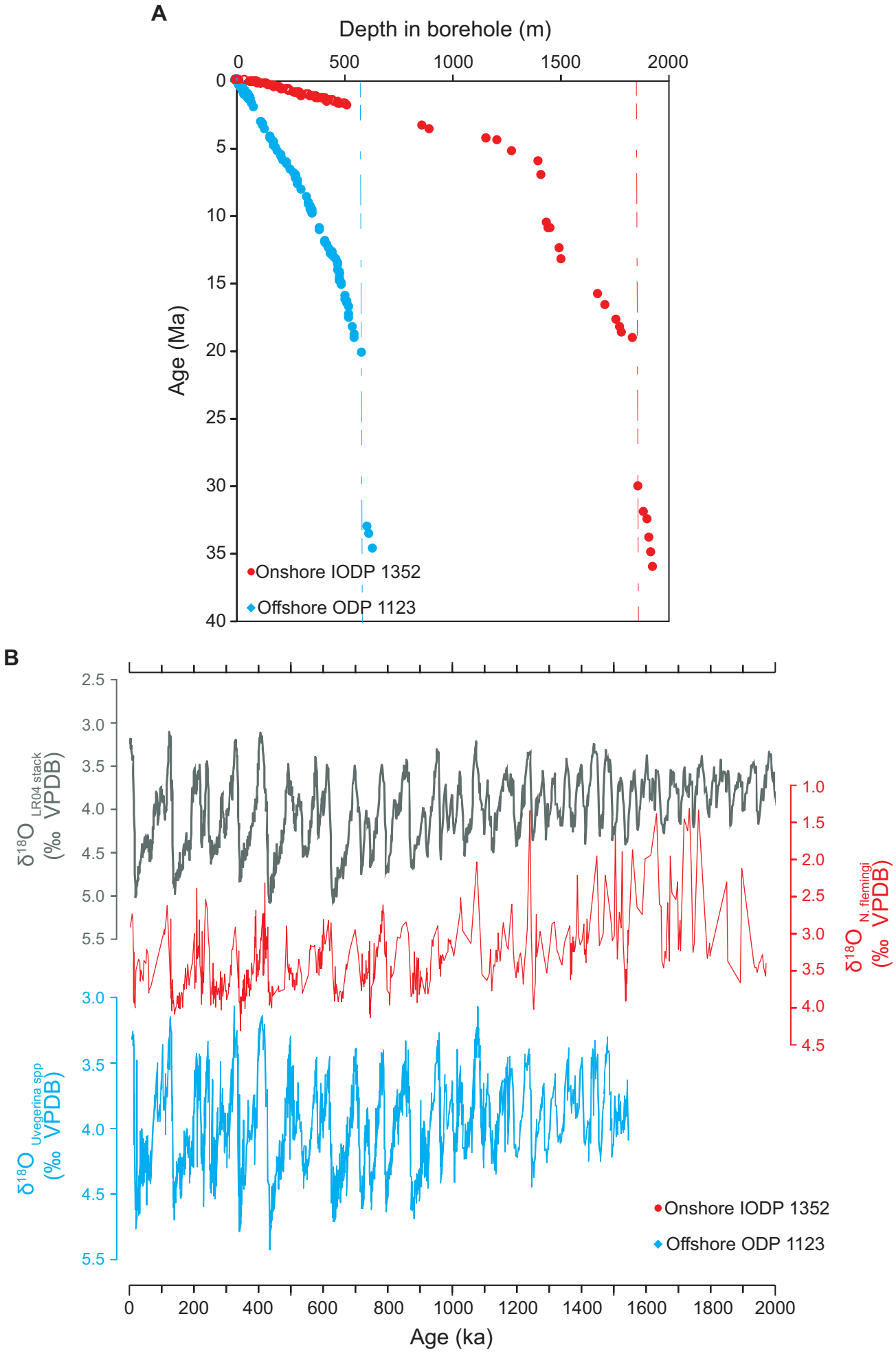
A
Depth in borehole (m)
0
500
1000
1500
2000
0
5
10
15
20
25
30
35
40
Age (Ma)
Onshore IODP 1352
Offshore ODP 1123
B
δ18O LR04 stack (‰ VPDB)
2.5
3.0
3.5
4.0
4.5
5.0
5.5
δ18O N. flemingi (‰ VPDB)
1.0
1.5
2.0
2.5
3.0
3.5
4.0
4.5
δ18O Uvegerina spp (‰ VPDB)
3.0
3.5
4.0
4.5
5.5
Onshore IODP 1352
Offshore ODP 1123
0
200
400
600
800
1000
1200
1400
1600
1800
2000
Age (ka)

Fig. S1. Age model construction. (**A**) Time (Ma) versus depth in borehole (m), using chronostratigraphic information (*36-38*). Dashed vertical lines show the location of the Marshall Paraconformity. (**B**) Oxygen isotope records. The reference benthic $\delta^{18}O$ record LR04 (*32*) is shown in black at the top. The planktonic foraminifera (*N. flemingi*) $\delta^{18}O$ record from the offshore IODP 1352 borehole (*37, 38*) is shown in red in the middle. The planktonic foraminifera (*Uvegerina spp*) $\delta^{18}O$ record from the onshore ODP 1123 borehole (*36*) is shown in blue at the bottom.

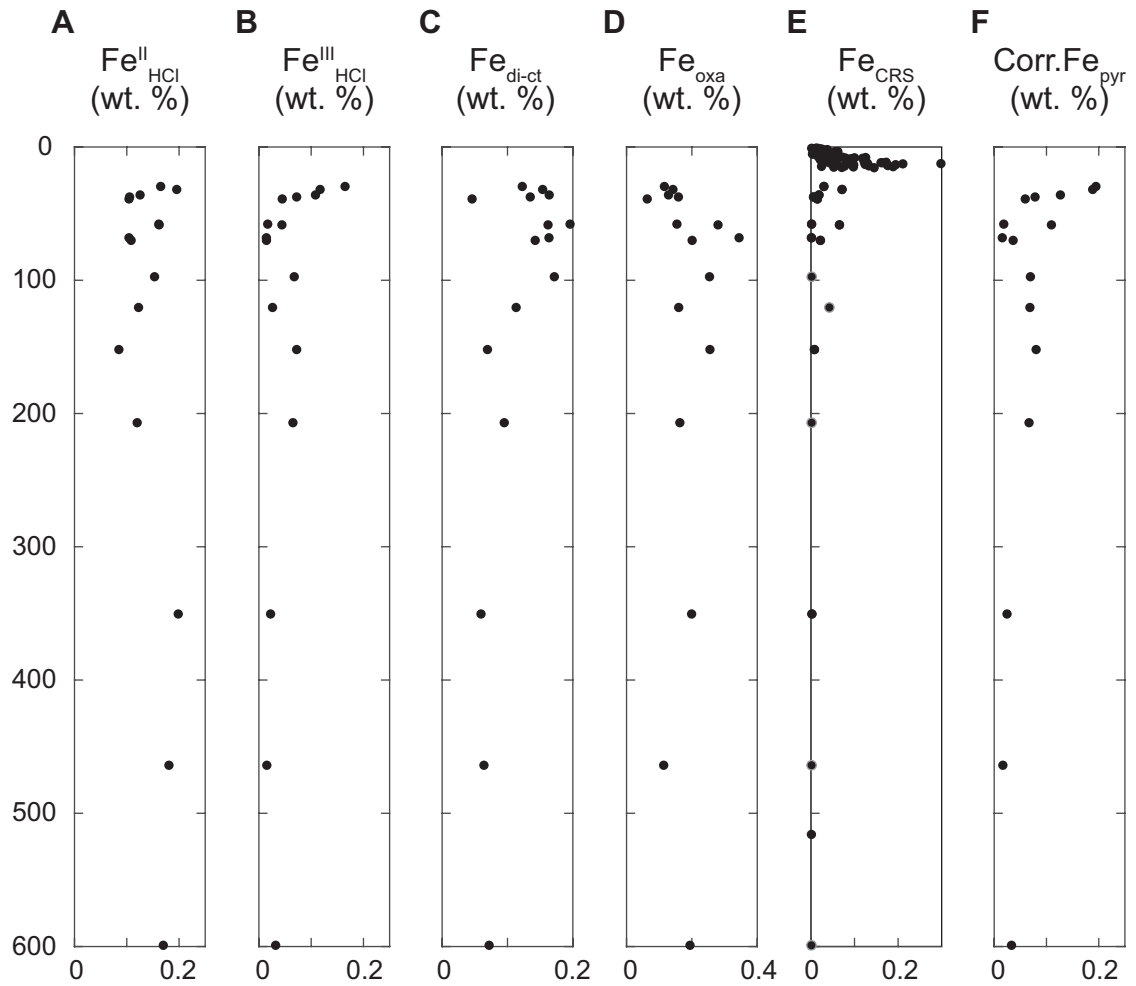

Fig. S2. Variations in wt.% of highly reactive Fe in the deep core. (**A**) HCl-extracted Fe^{II} (Fe^{II}_{HCl}) represents unsulfidized Fe^{II}. (**B**) HCl-extracted Fe^{III} (Fe^{III}_{HCl}) represents metastable Fe^{III} hydroxides, interpreted here to reflect post-coring oxidation of AVS and pyrite. (**C**) Dithionite-extracted Fe^{III} (Fe_{di-ct}) represents crystalline Fe^{III} (oxyhydr)oxides. (**D**) Oxalate-extracted Fe (Fe_{oxa}) represents magnetite. (**E**) Chromium-reducible S-bound Fe^{II} (Fe_{CRS}) represents pyrite; (**F**) The iron sulfide pool (pyrite + AVS) prior to post-sampling oxidation ($Corr.Fe_{pyr}$), determined by adding Fe^{III}_{HCl} and Fe_{CRS} (see Materials and Methods for details).

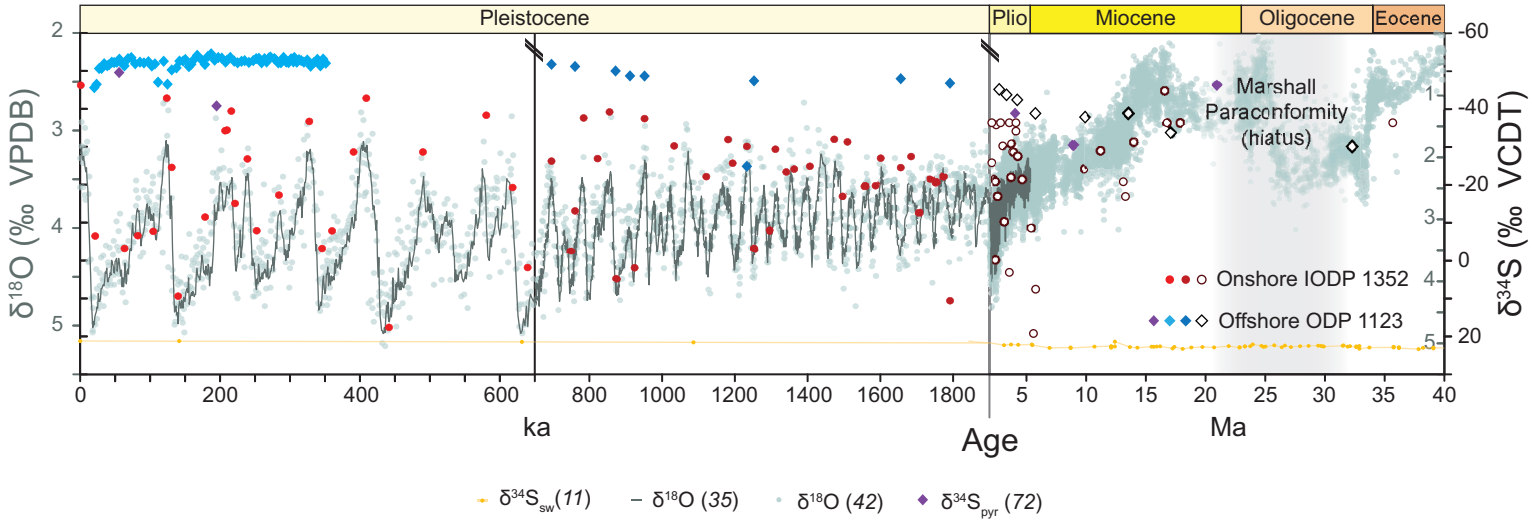

Fig. S3. Shelf and deep basin pyrite $\delta^{34}S$ values (red and blue, respectively, this study) and interpolated $\delta^{34}S$ values of seawater sulfate (yellow; ref. *11*) over the last 40 Myr. Filled markers have strong stratigraphic age constraints (foraminiferal $\delta^{18}O$ measurements), whereas empty markers have less robust age constraints (biostratigraphic and/or magnetostratigraphic tie-points). Also shown in purple are previously published $\delta^{34}S$ values of total reduced inorganic sulfur (TRIS, ref. *71*). For global climatic context, deep-sea records of $\delta^{18}O$ (*34, 41*; light circles and dark line, respectively) are shown. Note the change of scale of $\delta^{18}O$ associated with the change of timescale between the middle and rightmost parts of the figure, shown as the inner gray y axis on the right.

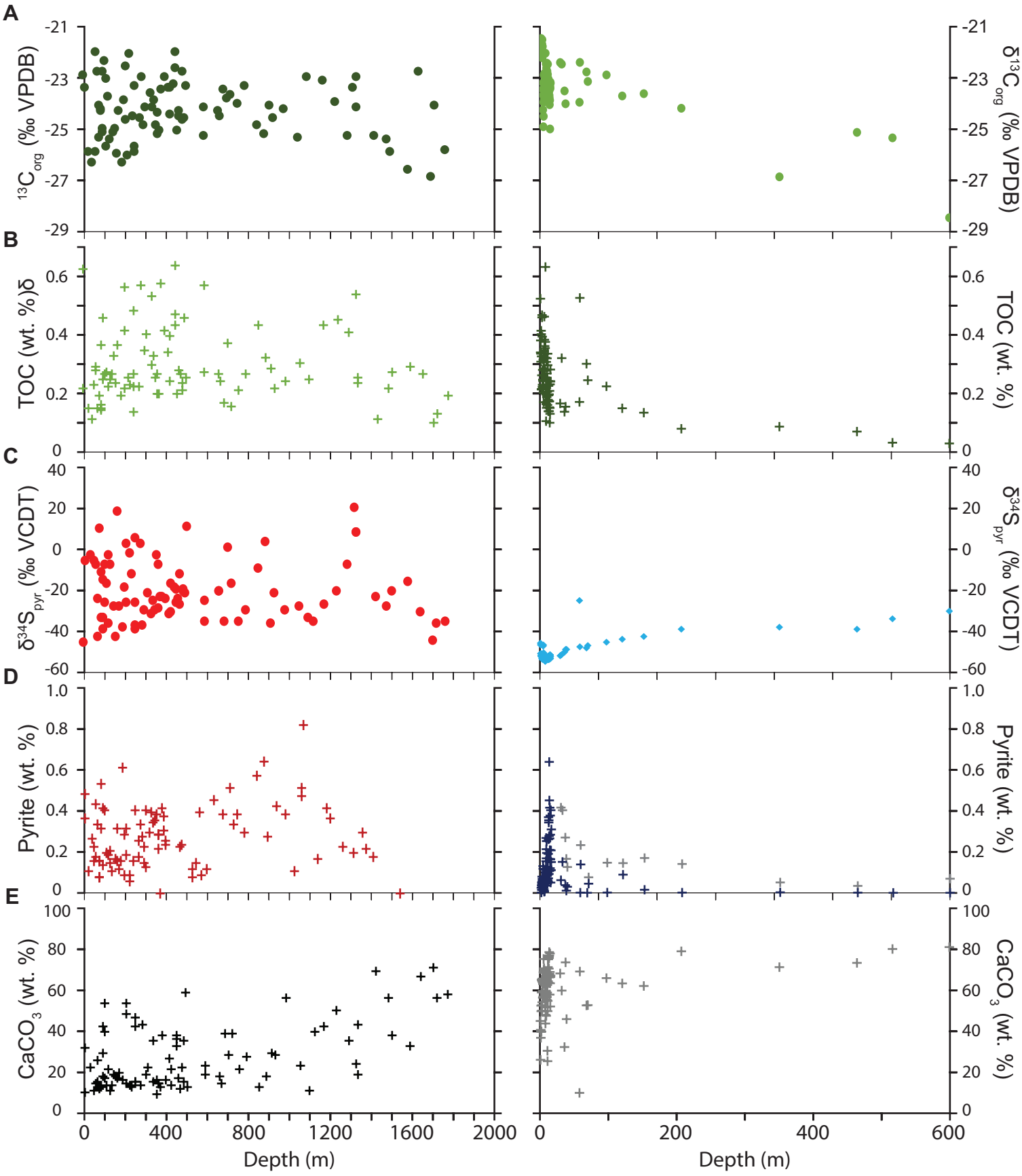

Fig. S4. Depth profiles of geochemical records for IODP 1352 (left) and ODP 1123 (right). (**A**) $\delta^{13}C_{org}$; (**B**) Total organic carbon (TOC); (**C**) $\delta^{34}S_{pyr}$; (**D**) Pyrite content (uncorrected in dark blue, corrected in grey); (**E**) Calcium carbonate content ($CaCO_3$).

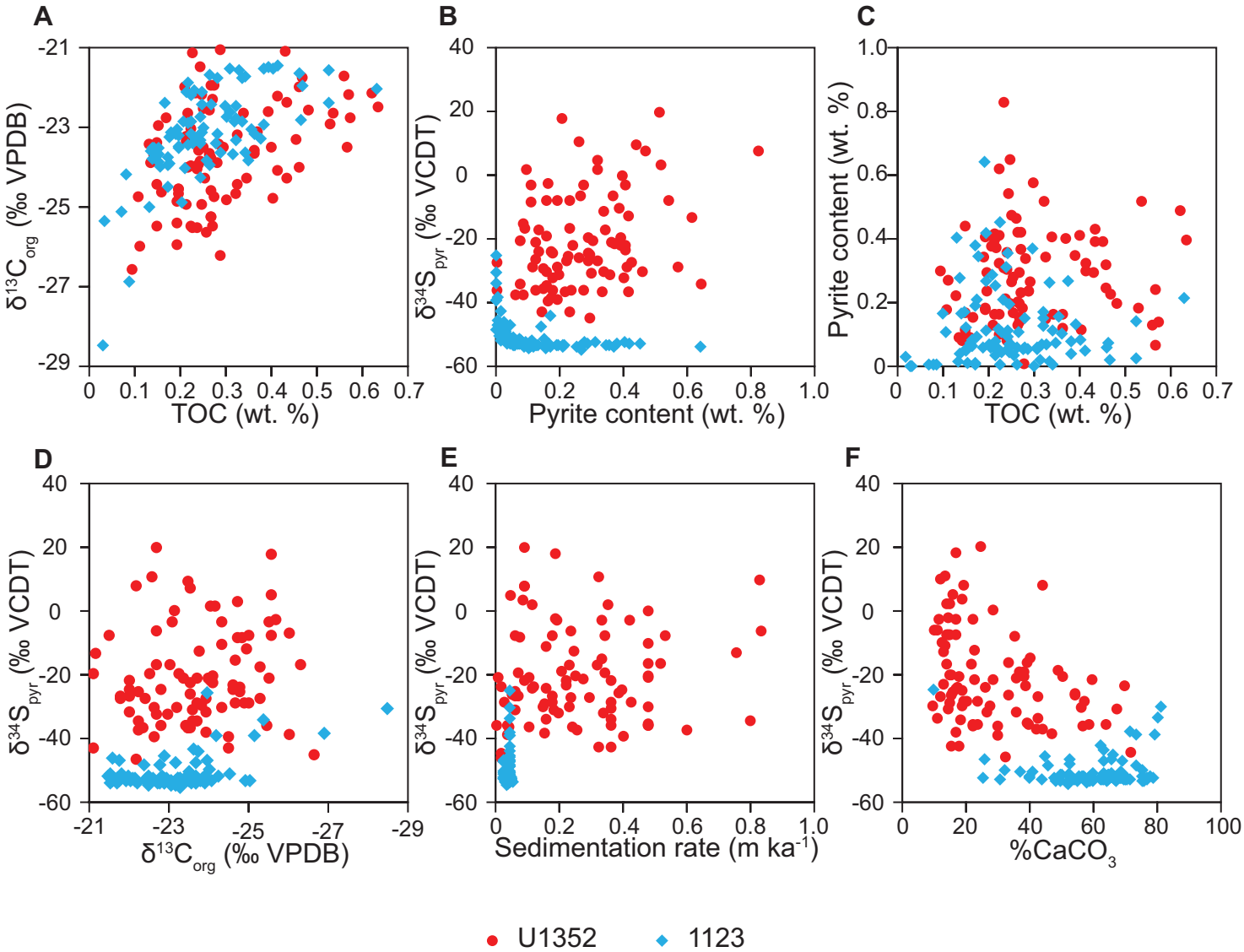

Fig. S5. Scatter plots of geochemical data. (**A**) $\delta^{13}C_{org}$ vs. total organic carbon (TOC); (**B**) $\delta^{34}S_{pyr}$ vs. uncorrected pyrite content; (**C**) Uncorrected pyrite content vs. TOC; (**D**) $\delta^{34}S_{pyr}$ vs. $\delta^{13}C_{org}$, (**E**) $\delta^{34}S_{pyr}$ vs. sedimentation rate (m ky^{-1}); (**F**) $\delta^{34}S_{pyr}$ vs. calcium carbonate content.

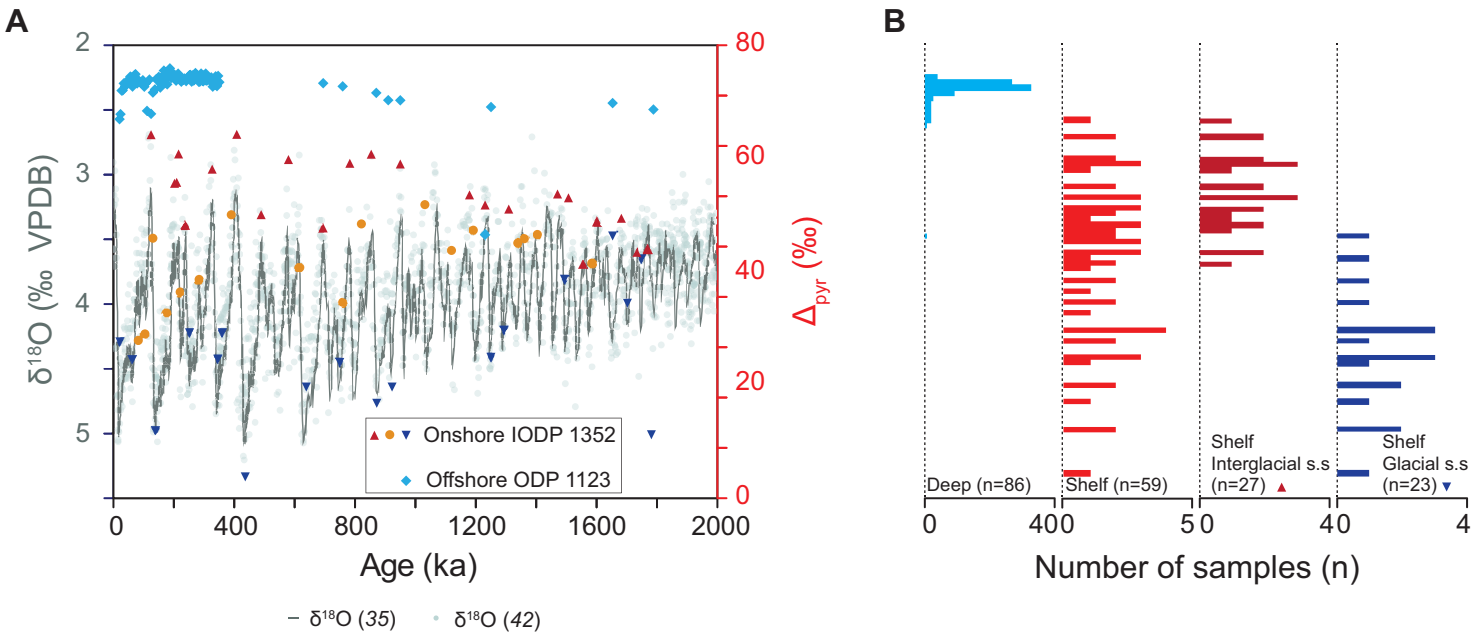

Fig. S6. Glacial – Interglacial bimodal distribution. (A) Shelf and basin Δ_{pyr} over the last 2 Myr. Glacial *sensu stricto*, interglacial *sensu stricto* and intermediate data from the shelf core are shown in dark blue upside-down triangles, dark red triangles and orange circles, respectively. Data from the basinal core are shown in light blue diamonds. For global climatic context, deep-sea records of $\delta^{18}O$ (*34, 41*) are show in the dark line and light gray circles. **(B)** Histograms of $\delta^{34}S_{pyr}$ in the basinal (light blue) and shelf (red) boreholes. The shelf data are further divided into interglacial *sensu stricto* (dark red) and glacial *sensu stricto* (dark blue).

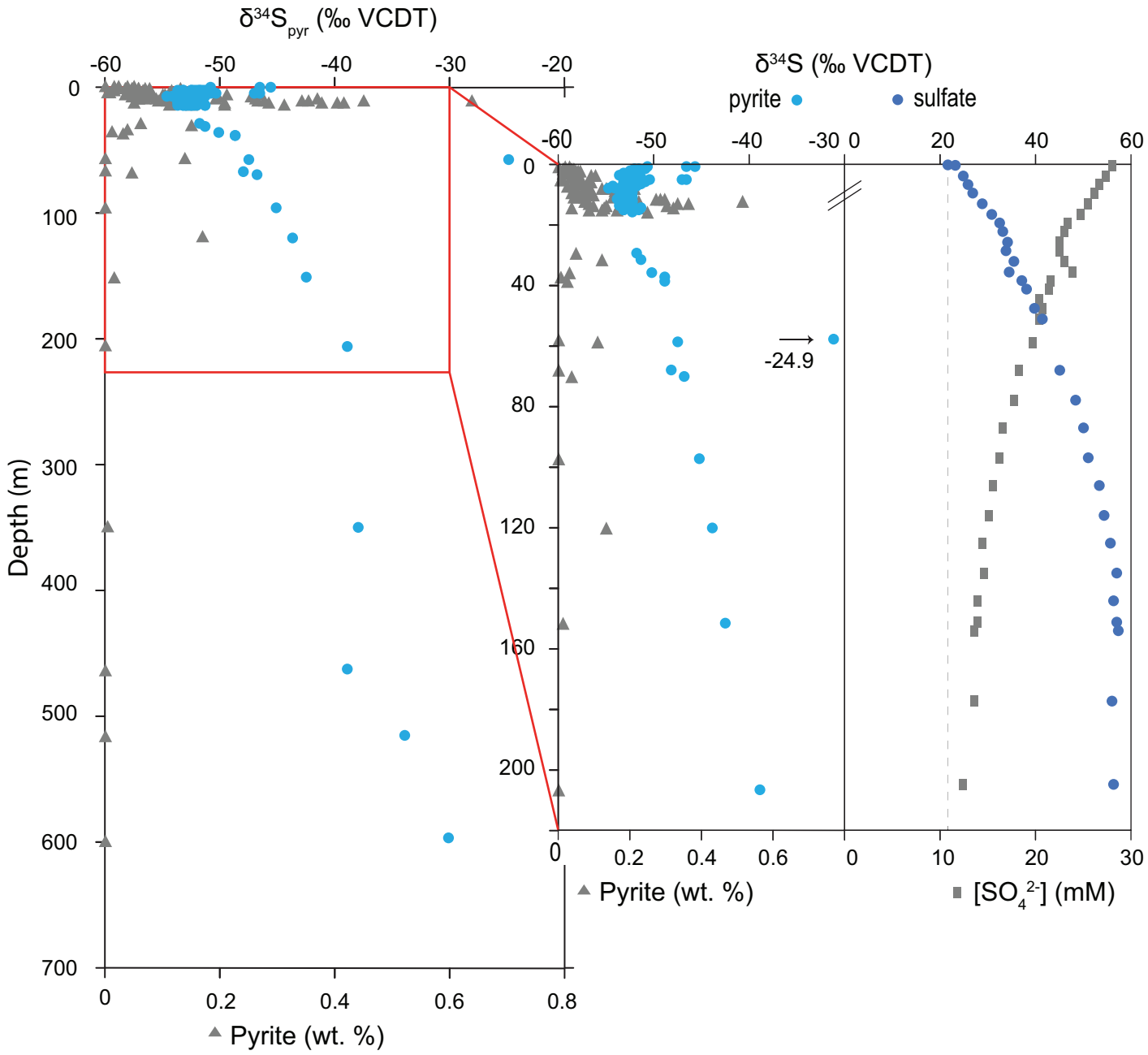

Fig. S7. Concentration and $\delta^{34}S$ depth profiles of porewater sulfate and pyrite in the offshore ODP borehole 1123. Porewater sulfate data are from ref. *53*.

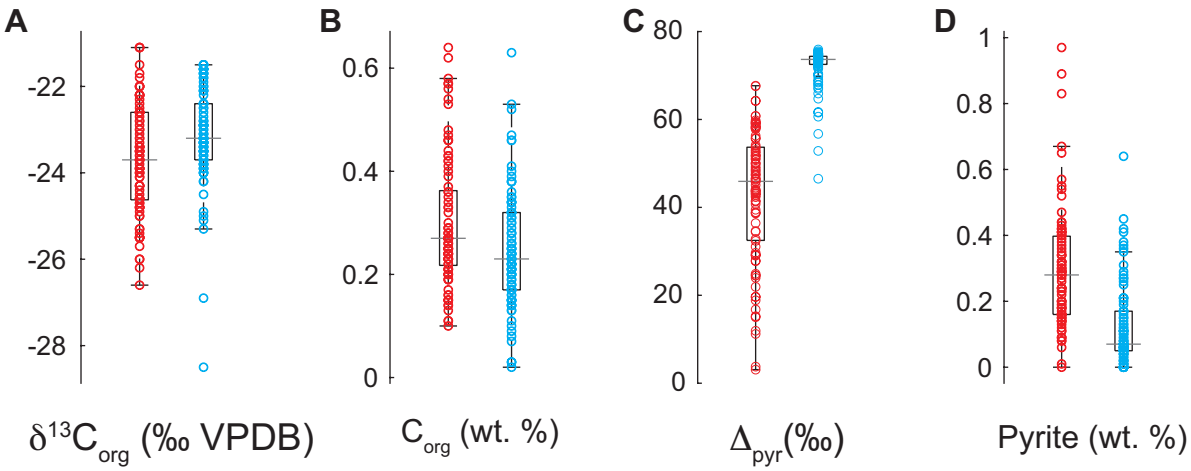

Fig. S8. Box and whisker plots. (**A**) $\delta^{13}C_{org}$, (**B**) TOC, (**C**) Δ_{pyr} and (**D**) Uncorrected pyrite content. The horizontal lines in the box middles denote the median, the box boundaries denote the 25th and 75th percentiles, and the vertical ranges shown by dashed lines ending in tick marks contain 99.3% of the data.

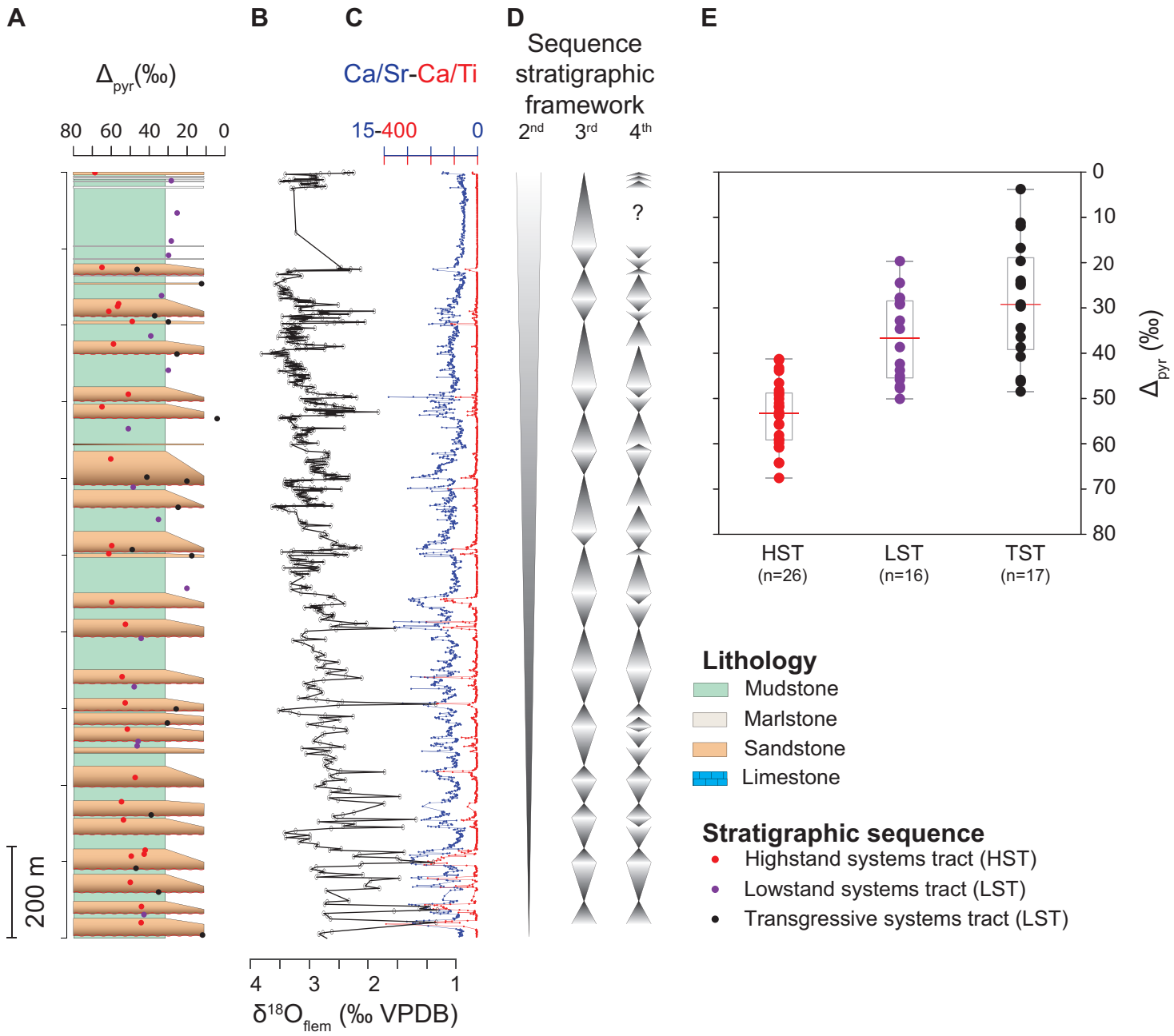

Fig. S9. Δ_{pyr} and sea level dependence. (**A**) Stratigraphy in the upper 500 m of IODP borehole 1352. (**B**) $\delta^{18}O$ of benthic foraminifera (*N. flemingi sp.*) downcore variations (*32*, *31*). (**C**) XRF Ca/Sr (blue) and Ca/Ti (red) ratios (*37*). (**D**) Sequence stratigraphic framework. (**E**) Box and whisker plots of Δ_{pyr} values grouped by systems tract associated with 4th order sea-level variation. Red horizontal lines denote the median, the box upper and lower boundaries denote the 75th and 25th percentile of the data, and the black horizontal lines contain 99.3% of the data.

GEOCHEMICAL RESULTS OF IODP 317 - SITE 1352 & ODP 181 - SITE 1123

Depth in borehole	Age	$CaCO_3$	$\delta^{15}N$	TN	$\delta^{13}C_{org}$	TOC	$\delta^{34}S_{pyr}$	FeS_2	Δ_{pyr}
(mbsf)	(Ma)	(wt. %)	(‰ VAIR)	(wt. %)	(‰ VPDB)	(wt. %)	(‰ VCDT)	(wt. %)	(‰ VCDT)
IODP 317 - SITE 1352									
0.02	0.00	33	7.1	0.09	-22.2	0.62	-46.3	0.29	67.6
6.00	0.02	11	4.4	0.12	-22.6	0.22	-6.5	0.40	27.8
27.20	0.06	23	4.6	0.10	-25.5	0.15	-3.2	0.11	24.5
46.28	0.08	11	ND	0.02	-26.0	0.11	-6.6	0.27	27.9
55.38	0.10	15	4.0	0.03	-25.5	0.23	-7.7	0.16	29.0
62.98	0.12	15	4.4	0.15	-21.1	0.29	-42.9	0.28	64.2
64.36	0.13	26	4.7	0.13	-22.0	0.28	-24.6	0.18	45.9
73.50	0.14	12	4.0	0.12	-23.4	0.15	9.4	0.47	11.9
81.00	0.18	13	4.1	0.03	-24.9	0.19	-11.5	0.34	32.8
86.50	0.21	43	5.3	0.02	-23.7	0.14	-34.3	0.08	55.6
89.00	0.21	19	4.7	0.04	-23.6	0.36	-34.5	0.16	55.8
92.00	0.22	30	4.6	0.01	-24.5	0.15	-39.5	0.16	60.8
94.13	0.22	41	5.0	0.02	-24.6	0.16	-15.1	0.09	36.4
97.99	0.24	55	5.2	0.12	-22.0	0.46	-26.9	0.32	48.2
99.00	0.25	17	4.1	0.11	-21.5	0.25	-7.9	0.54	29.2
108.00	0.28	14	3.6	0.03	-25.3	0.27	-17.3	0.14	38.6
113.60	0.33	22	4.6	0.10	-22.3	0.27	-36.8	0.42	58.1
121.00	0.35	12	4.2	0.13	-23.0	0.23	-3.2	0.44	24.6
130.16	0.36	14	3.9	0.03	-25.0	0.25	-7.9	0.20	29.2
145.98	0.39	19	3.8	0.03	-24.6	0.27	-28.7	0.19	50.1
154.01	0.41	18	3.6	0.03	-24.4	0.33	-42.9	0.15	64.3
161.50	0.44	17	3.4	0.03	-25.5	0.24	17.6	0.41	3.8
168.10	0.49	21	4.5	0.04	-23.7	0.36	-28.7	0.12	50.1
187.62	0.58	17	4.1	0.02	-26.0	0.19	-38.4	0.18	59.8
200.00	0.62	49	4.6	0.02	-23.2	0.21	-19.3	0.16	40.8
203.00	0.64	15	4.1	0.04	-24.1	0.42	1.8	0.32	19.6
206.60	0.70	54	5.2	0.15	-21.7	0.56	-26.3	0.14	47.7
219.00	0.75	15	3.5	0.03	-25.7	0.26	-2.5	0.17	24.0
228.00	0.76	13	4.5	0.15	-21.1	0.23	-13.2	0.67	34.6
245.02	0.78	42	4.9	0.02	-23.9	0.14	-37.7	0.09	59.2
248.00	0.82	16	3.7	0.03	-25.3	0.27	-27.0	0.29	48.4
249.49	0.86	47	5.6	0.04	-22.6	0.48	-39.3	0.20	60.8
250.60	0.87	16	3.7	0.03	-25.5	0.23	4.7	0.32	16.8
272.35	0.92	14	3.9	0.15	-24.0	0.23	1.9	0.97	19.7
280.74	0.95	44	4.6	0.17	-22.2	0.57	-37.5	0.06	59.0
295.50	1.03	19	4.0	0.04	-24.3	0.35	-30.3	0.16	51.8
305.60	1.12	23	4.6	0.04	-23.5	0.40	-22.2	0.41	43.8

330.10	1.18	36	4.5	0.15	-22.9	0.53	-32.0	0.19	53.6
336.00	1.19	16	4.0	0.03	-23.5	0.29	-25.7	0.26	47.3
347.00	1.23	10	3.9	0.16	-23.2	0.33	-30.2	0.34	51.8
351.60	1.25	17	4.0	0.03	-24.3	0.26	-3.3	0.28	24.9
361.00	1.30	15	3.2	0.03	-24.7	0.20	-8.0	0.24	29.7
364.00	1.31	15	3.6	0.03	-23.8	0.27	-29.4	0.15	51.1
372.00	1.34	13	3.4	0.03	-24.6	0.20	-23.4	0.41	45.1
375.25	1.36	39	5.0	0.15	-22.8	0.58	-24.2	0.14	45.8
396.00	1.41	17	4.1	0.16	-22.2	0.42	-24.9	0.30	46.6
412.20	1.47	27	3.8	0.04	-22.6	0.34	-32.1	0.40	53.7
421.00	1.50	22	4.6	0.05	-22.6	0.39	-17.0	0.35	38.7
424.00	1.51	14	3.7	0.03	-23.9	0.24	-31.4	0.36	53.1
443.50	1.56	37	4.4	0.14	-22.5	0.64	-19.6	0.44	41.3
446.28	1.59	39	3.7	0.04	-21.1	0.43	-19.8	0.29	41.5
447.57	1.60	33	4.3	0.17	-21.8	0.47	-27.1	0.24	48.8
455.38	1.66	18	3.7	0.03	-24.6	0.20	-24.6	0.29	46.3
463.57	1.68	12	3.8	0.03	-23.9	0.28	-27.5	0.00	49.2
469.74	1.71	23	4.1	0.03	-23.7	0.27	-12.7	0.42	34.4
480.00	1.74	36	4.0	0.02	-22.0	0.21	-21.5	0.38	43.3
484.76	1.75	16	3.3	0.03	-24.1	0.24	-20.6	0.31	42.3
490.00	1.77	60	3.7	0.13	-24.0	0.46	-22.1	0.24	43.9
498.01	1.79	14	3.8	0.14	-22.6	0.25	10.6	0.29	11.2
583.00	2.88	19	3.0	0.14	-24.8	0.27	-25.5	0.23	47.4
587.99	2.89	24	ND	ND	-23.5	0.57	-36.3	0.24	58.2
657.97	3.01	18	3.0	0.15	-23.7	0.27	-21.1	0.14	43.1
661.10	3.01	15	3.6	0.14	-23.9	0.24	-20.8	0.08	42.7
679.80	3.05	39	3.6	0.02	-22.8	0.17	-35.8	0.15	57.8
700.90	3.08	29	3.1	0.14	-23.1	0.37	0.1	0.40	21.9
716.00	3.11	40	3.1	0.02	-23.0	0.16	-16.9	0.09	38.9
749.73	3.17	22	2.8	0.02	-23.4	0.21	-36.0	0.13	58.0
788.85	3.24	28	2.9	0.03	-22.6	0.26	-30.3	0.20	52.4
846.17	3.33	13	3.0	0.15	-24.3	0.44	-10.3	0.31	32.4
882.21	3.67	19	2.9	0.14	-24.7	0.32	3.3	0.52	18.9
905.40	3.75	30	2.9	0.03	-23.4	0.28	-36.4	0.34	58.5
926.27	3.79	29	2.8	0.03	-24.0	0.22	-21.9	0.39	44.1
978.00	3.91	56	2.6	0.02	-23.6	0.24	-30.5	0.30	52.7
1049.33	4.08	24	2.7	0.03	-24.8	0.30	-28.7	0.57	50.9
1092.83	4.18	11	2.2	0.12	-22.2	0.25	-34.0	0.65	56.3
1114.95	4.23	40	2.6	0.11	ND	ND	-36.1	0.28	58.4
1165.44	4.37	43	2.4	0.13	-22.4	0.43	-27.5	0.43	49.8
1227.49	4.84	50	2.7	0.13	-23.3	0.46	-21.1	0.42	43.6
1283.90	5.45	36	2.9	0.12	-24.8	0.41	-8.5	0.11	31.1
1317.79	5.75	25	2.0	0.12	-22.7	0.54	19.6	0.55	3.1
1327.00	5.83	44	1.9	0.02	-23.5	0.25	7.5	0.89	15.2
1330.40	5.86	20	2.1	0.10	-22.2	0.24	7.7	0.83	15.0

1419.03	9.92	70	3.0	0.01	-24.8	0.11	-23.9	0.18	46.6
1477.75	11.50	57	3.1	0.02	-25.0	0.21	-28.9	0.41	51.5
1496.48	13.33	38	3.4	0.02	-25.5	0.27	-20.9	0.37	43.7
1577.55	13.46	33	2.6	0.09	-26.2	0.29	-16.7	0.23	39.5
1637.70	14.25	68	3.1	0.10	-22.0	0.27	-31.3	0.20	54.2
1697.33	16.70	72	2.8	0.01	-26.6	0.10	-44.8	0.30	67.7
1714.39	17.03	57	3.9	0.09	-23.4	0.13	-36.5	0.22	59.4
1760.66	18.04	59	3.3	0.02	-25.4	0.19	-36.0	0.18	59.0
1924.24	36.00	64	ND	ND	ND	ND	-36.3	0.01	59.4

ODP 181 - SITE 1123

0.76	0.02	45	ND	0.07	-21.6	0.52	-45.7	0.03	66.9
0.94	0.02	26	ND	0.05	-21.7	0.34	-46.6	0.00	67.8
1.14	0.03	41	ND	0.05	-21.5	0.38	-50.7	0.04	72.0
1.34	0.03	37	ND	0.05	-21.8	0.34	-50.8	0.02	72.0
1.54	0.03	40	ND	0.06	-21.6	0.31	-52.0	0.05	73.3
1.78	0.04	52	ND	0.06	-21.5	0.41	-51.5	0.05	72.7
1.94	0.04	50	ND	0.06	-21.5	0.40	-51.8	0.08	73.0
2.14	0.05	40	ND	0.03	-21.9	0.21	-52.4	0.04	73.7
2.33	0.05	59	ND	0.04	-21.6	0.33	-52.3	0.07	73.6
2.54	0.05	65	ND	0.04	-22.1	0.21	-52.4	0.06	73.7
2.74	0.06	65	ND	0.03	-21.7	0.26	-53.2	0.06	74.5
3.04	0.06	53	ND	0.05	-21.7	0.46	-51.8	0.06	73.1
3.14	0.06	50	ND	0.07	-22.0	0.47	-51.4	0.02	72.7
3.38	0.07	54	ND	0.05	-21.5	0.39	-53.3	0.13	74.6
3.54	0.07	64	ND	0.04	-22.2	0.22	-53.6	0.12	74.9
3.73	0.08	66	ND	0.02	-22.1	0.23	-52.0	0.05	73.3
3.96	0.09	60	ND	0.04	-21.8	0.28	-52.4	0.06	73.7
4.14	0.09	56	ND	0.04	-22.1	0.25	-52.2	0.07	73.5
4.34	0.10	63	ND	0.04	-23.4	0.22	-52.6	0.08	73.8
4.49	0.10	63	ND	0.04	-24.2	0.24	-51.4	0.05	72.7
4.63	0.11	57	ND	0.04	-23.2	0.22	-52.0	0.05	73.2
4.77	0.11	63	ND	0.05	-23.7	0.32	-47.1	0.02	68.4
5.02	0.12	69	ND	0.04	-24.9	0.20	-52.7	0.07	73.9
5.19	0.12	66	ND	0.04	-23.9	0.26	-46.6	0.01	67.9
5.38	0.13	75	ND	0.03	-24.5	0.17	-50.4	0.01	71.6
5.59	0.14	69	ND	0.03	-23.7	0.29	-50.9	0.05	72.2
5.79	0.14	69	ND	0.04	-22.9	0.32	-52.7	0.07	74.0
6.03	0.15	71	ND	0.05	-23.8	0.35	-52.7	0.07	74.0
6.18	0.15	70	ND	0.03	-23.6	0.34	-53.1	0.11	74.4
6.42	0.16	65	ND	0.04	-22.8	0.46	-51.2	0.07	72.5
6.58	0.16	65	ND	0.04	-22.9	0.38	-51.8	0.08	73.1
6.78	0.16	69	ND	ND	ND	ND	-53.2	0.10	74.5
6.98	0.17	58	ND	0.04	-23.2	0.36	-54.2	0.10	75.5
7.30	0.17	62	ND	0.05	-23.4	0.28	-52.9	0.05	74.2

7.50	0.18	64	ND	0.03	-23.8	0.26	-51.8	0.04	73.1
7.70	0.18	52	ND	0.04	-23.1	0.35	-54.0	0.16	75.2
7.90	0.19	52	ND	0.04	-23.3	0.38	-54.6	0.27	75.9
8.10	0.19	44	ND	0.09	-22.0	0.63	-52.9	0.21	74.2
8.30	0.20	48	ND	0.05	-23.3	0.32	-53.6	0.17	74.9
8.50	0.20	60	ND	0.04	-22.9	0.21	-53.5	0.25	74.8
8.71	0.21	62	ND	0.04	-23.2	0.20	-52.4	0.11	73.7
8.80	0.21	63	ND	0.04	-22.4	0.25	-52.9	0.20	74.2
8.98	0.21	67	ND	ND	ND	0.11	-53.7	0.11	75.0
9.20	0.22	48	ND	ND	ND	0.16	-52.7	0.08	74.0
9.39	0.23	55	ND	0.05	-22.6	0.31	-52.3	0.06	73.6
9.60	0.23	57	ND	0.05	-23.0	0.25	-52.6	0.07	73.9
9.77	0.24	69	ND	0.03	-23.5	0.15	-52.8	0.05	74.1
10.00	0.24	68	ND	0.03	-23.2	0.19	-52.4	0.06	73.7
10.24	0.25	57	ND	0.05	-22.4	0.27	-52.8	0.11	74.1
10.40	0.25	55	ND	0.05	-22.8	0.32	-53.4	0.13	74.7
10.60	0.26	59	ND	0.04	-22.7	0.24	-53.4	0.09	74.8
10.80	0.26	63	ND	0.03	-22.9	0.21	-52.3	0.06	73.6
11.02	0.26	30	ND	ND	ND	0.17	-53.3	0.19	74.7
11.18	0.27	25	ND	ND	ND	0.16	-52.5	0.07	73.8
11.36	0.27	50	ND	0.05	-22.9	0.34	-53.6	0.26	74.9
11.47	0.27	55	ND	0.05	-22.5	0.30	-53.8	0.37	75.1
11.76	0.28	71	ND	0.03	-23.1	0.18	-53.4	0.35	74.7
11.86	0.28	64	ND	0.02	-23.3	0.24	-53.0	0.36	74.4
12.06	0.28	75	ND	0.02	-23.3	0.18	-52.2	0.09	73.5
12.26	0.29	75	ND	0.02	-23.8	0.14	-52.3	0.28	73.6
12.46	0.29	76	ND	0.02	-23.0	0.19	-53.7	0.64	75.0
12.66	0.29	68	ND	0.03	-23.4	0.23	-52.5	0.45	73.8
12.86	0.30	63	ND	0.03	-23.3	0.23	-52.3	0.11	73.6
13.08	0.30	71	ND	0.02	-23.5	0.20	-53.3	0.27	74.6
13.28	0.30	77	ND	0.03	-23.5	0.20	-52.5	0.42	73.8
13.36	0.31	76	ND	0.02	-23.9	0.17	-53.7	0.21	75.0
13.58	0.31	79	ND	0.02	-23.5	0.14	-52.4	0.17	73.7
13.76	0.31	77	ND	0.02	-23.7	0.15	-53.1	0.12	74.4
13.96	0.32	68	ND	0.02	-23.8	0.17	-52.8	0.38	74.2
14.16	0.32	66	ND	0.03	-24.0	0.21	-52.4	0.29	73.8
14.36	0.32	58	ND	ND	ND	0.10	-53.0	0.17	74.3
14.56	0.33	69	ND	0.02	-23.9	0.15	-51.4	0.05	72.7
14.76	0.33	78	ND	0.02	-25.0	0.13	-52.4	0.41	73.7
14.96	0.34	63	ND	0.03	-23.3	0.23	-53.2	0.21	74.5
15.16	0.34	52	ND	0.04	-23.4	0.24	-51.4	0.11	72.8
15.36	0.35	66	ND	0.04	-23.2	0.28	-53.2	0.15	74.6
15.56	0.35	67	ND	0.04	-23.2	0.24	-52.1	0.31	73.5
29.61	0.70	68	ND	0.03	-22.4	0.17	-51.9	0.06	73.3
31.87	0.76	60	ND	0.05	-22.5	0.32	-51.3	0.15	72.7

35.98	0.87	32	ND	0.02	-23.5	0.14	-50.1	0.04	71.6
37.50	0.91	74	ND	0.02	-24.0	0.15	-48.8	0.01	70.3
38.99	0.95	46	ND	ND	ND	0.02	-48.8	0.03	70.3
57.88	1.23	10	ND	0.03	-24.0	0.17	-24.9	0.00	46.5
58.44	1.25	69	ND	0.08	-22.4	0.53	-47.5	0.14	69.1
68.12	1.66	53	ND	0.05	-22.8	0.30	-48.1	0.00	69.8
70.08	1.79	53	ND	0.04	-23.1	0.25	-46.9	0.05	68.6
97.36	2.72	66	ND	0.03	-22.9	0.22	-45.2	0.00	67.2
120.43	3.33	63	ND	0.02	-23.7	0.15	-43.8	0.17	65.9
152.00	4.23	62	ND	0.02	-23.6	0.13	-42.5	0.02	64.7
206.90	5.75	79	ND	0.01	-24.2	0.08	-38.9	0.00	61.6
350.45	9.92	71	ND	0.01	-26.9	0.09	-37.9	0.00	60.6
463.96	13.59	73	ND	0.01	-25.1	0.07	-38.9	0.00	61.7
515.89	17.09	80	ND	0.01	-25.3	0.03	-33.8	0.00	56.7
599.07	32.24	81	ND	0.01	-28.5	0.03	-30.1	0.00	52.8

Table S1. Depth, estimated age, and associated geochemical information of samples from the IODP 317 – site 1352 and ODP 181 – site 1123 boreholes.

FE SPECIATION RESULTS OF ODP 181 - SITE 1123

Cumul. depth in borehole	Age	Fe^{II}_{HCl}	Fe^{III}_{HCl}	$Fe_{di\text{-}ct}$	Fe_{oxa}	Fe_{CRS}	$Corr.Fe_{pyr}$
(mbsf)	(Ma)	(wt. %)	(wt. %)	(wt. %)	(wt. %)	(wt. %)	(wt. %)
ODP 181 - SITE 1123							
29.61	0.70	0.16	0.16	0.12	0.12	0.03	0.19
31.87	0.76	0.20	0.12	0.15	0.14	0.07	0.19
35.98	0.87	0.13	0.11	0.16	0.13	0.02	0.13
37.50	0.91	0.11	0.07	0.13	0.16	0.01	0.08
38.99	0.95	0.10	0.04	0.05	0.06	0.01	0.06
57.88	1.23	0.16	0.02	0.20	0.15	0.00	0.02
58.44	1.25	0.16	0.04	0.16	0.28	0.07	0.11
68.12	1.66	0.10	0.01	0.16	0.34	0.00	0.02
70.08	1.79	0.11	0.01	0.14	0.20	0.02	0.04
97.36	2.72	0.15	0.07	0.17	0.25	0.00	0.07
120.43	3.33	0.12	0.03	0.11	0.16	0.04	0.07
152.00	4.23	0.08	0.07	0.07	0.26	0.01	0.08
206.90	5.75	0.12	0.07	0.10	0.16	0.00	0.07
350.45	9.92	0.20	0.02	0.06	0.20	0.00	0.02
463.96	13.59	0.18	0.02	0.06	0.11	0.00	0.02
599.07	32.24	0.17	0.03	0.07	0.19	0.00	0.03

Table S2. Variations in wt.% of highly reactive Fe from the ODP 181 – site 1123 deep borehole.

DIGITIZATION OF BÖTTCHER ET AL. (2004) DATASET		
Digitalization n°	Cumul. depth in borehole (mbsf)	$\delta^{34}S_{TRIS}$ (‰)
SAMPLE 1		
1	3.1	-49.60
2	2.97	-49.5
3	2.36	-49.6
Mean	2.8±0.4	-49.6±0.06
Age (Ma)	0.06±0.01	
SAMPLE 2		
1	9.1	-40.7
2	8.7	-40.8
3	8.43	-40.8
Mean	8.7±0.3	-40.8±0.06
Age (Ma)	0.21±0.01	
SAMPLE 3		
1	147	-38.9
2	146	-38.9
3	145	-39
Mean	146.0±1.0	-38.9±0.06
Age (Ma)	4.05±0.04	
SAMPLE 4		
1	324	-30.5
2	324	-30.5
3	323	-30.5
Mean	323.7±0.6	-30.5±0
Age (Ma)	8.87±0.03	
SAMPLE 5		
1	580	-46.3
2	581	-46.3
3	581	-46.3
Mean	580.7±0.6	-46.3±0
Age (Ma)	20.96±0.5	

Table S3. Previously reported total reducible inorganic sulfur (TRIS) $\delta^{34}S$ values. Data are from on-board sulfur isotopic analysis (*71*).

Period	Sea-level fluctuation (m)	Age (Ma)	Depositional environment	$\delta^{34}S_{pyr}$ (‰) min	max	$\delta^{34}S_{pyr}$ amplitude changes (‰)	Reference
Plio-Pleistocene	50 to 150 m	<1.9	Shelf	-46	20	**66**	This study
		<0.02	Shelf	-38	15	**53**	*15*
		<0.5	Shelf	-44	32	**76**	*16*
		<0.4	Shelf	-34	33	**67**	*76*
		<0.5	Shelf - OMZ	-32	-5	**27**	*77*
End Permian mass extinction (EPME)	2nd and 3rd (ref. *78*)	252	Shelf	-21	47	**68**	*19*
			Platform	-23	2	**25**	*79*
			Platform	-38	12	**50**	*80*
			Shelf	-40	3	**43**	*81*
			shelf	0	22	**22**	*81*
			Shelf	-40	0	**40**	*82*
			Shelf	-42	-15	**27**	*83*
Frasnian-Famennian Mass Extinction (Late Devonian)	2nd and 3rd (ref. *84*)	360 to 376	Shelf	-14	13	**27**	*85*
			Shelf	-10	35	**45**	*86*
			Shelf	-10	20	**30**	*87*
			Shelf	10	30	**20**	*88*
			Shelf	-14	20	**34**	*88*
Silurian Ireviken event	3rd and 4th (ref. *89*)	431	Platform	-25	45	**70**	*58*
			Platform	-25	45	**70**	*17*
Hirnantian positive Carbon Isotopic Excursion (HICE)	~125 m (ref. *90*)	443	Platform	-22	5	**27**	*57*
			Platform	-25	22	**47**	*91*
			Platform	-25	18	**43**	*92*
			Shelf	-32	20	**52**	*92*
			Shelf	-25	25	**50**	*93*
			Shelf	-30	10	**40**	*94*
Steptoean Positive Isotopic Carbon Excursion (SPICE)	Stratigraphic evidence (ref. *95*)	500	Shelf	-20	60	**80**	*96*
			Shelf	-10	55	**65**	*96*
			Shelf	-10	30	**40**	*96*
			Shelf	-11	-28	**17**	*97*

Table S4. Examples of Phanerozoic periods with high-amplitude $\delta^{34}S_{pyr}$ stratigraphic variations and variations in sea level. With large uncertainties, 2nd and 3rd-order sea-level variations of hundreds of meters over 0.5 to 5 Ma duration, whereas 3rd and 4th-order variations span between 0.01 to 0.5 Ma with sea-level amplitude from tens to hundreds of meters (*78, 98*). For the SPICE event, stratigraphic evidence suggests 25 to 50 m of sea-level variation (*78, 95*).

REFERENCES AND NOTES

1. R. A. Berner, Sedimentary pyrite formation—An update. *Geochim. Cosmochim. Acta* **48**, 605–615 (1984).

2. D. E. Canfield, J. Farquhar, Animal evolution, bioturbation, and the sulfate concentration of the oceans. *Proc. Natl. Acad. Sci. U.S.A.* **106**, 8123–8127 (2009).

3. D. D. Adams, M. T. Hurtgen, B. B. Sageman, Volcanic triggering of a biogeochemical cascade during Oceanic Anoxic Event 2. *Nat. Geosci.* **3**, 201–204 (2010).

4. D. E. Canfield, A. Teske, Late Proterozoic rise in atmospheric oxygen concentration inferred from phylogenetic and sulphur-isotope studies. *Nature* **382**, 127–132 (1996).

5. D. A. Fike, J. P. Grotzinger, L. M. Pratt, R. E. Summons, Oxidation of the Ediacaran ocean. *Nature* **444**, 744–747 (2006).

6. B. C. Gill, T. W. Lyons, S. A. Young, L. R. Kump, A. H. Knoll, M. R. Saltzman, Geochemical evidence for widespread euxinia in the later Cambrian ocean. *Nature* **469**, 80–83 (2011).

7. M. L. Gomes, M. T. Hurtgen, B. B. Sageman, Biogeochemical sulfur cycling during Cretaceous oceanic anoxic events: A comparison of OAE1a and OAE2. *Paleoceanography* **31**, 233–251 (2016).

8. W. D. Leavitt, I. Halevy, A. S. Bradley, D. T. Johnston, Influence of sulfate reduction rates on the Phanerozoic sulfur isotope record. *Proc. Natl. Acad. Sci. U.S.A.* **110**, 11244–11249 (2013).

9. J. D. Owens, B. C. Gill, H. C. Jenkyns, S. M. Bates, S. Severmann, M. M. Kuypers, R. G. Woodfine, T. W. Lyons, Sulfur isotopes track the global extent and dynamics of euxinia during Cretaceous Oceanic Anoxic Event 2. *Proc. Natl. Acad. Sci. U.S.A.* **110**, 18407–18412 (2013).

10. M. R. Raven, D. A. Fike, M. L. Gomes, S. M. Webb, A. S. Bradley, H.-L. O. McClelland, Organic carbon burial during OAE2 driven by changes in the locus of organic matter sulfurization. *Nat. Commun.* **9**, 3409 (2018).

11. V. C. F. Rennie, G. Paris, A. L. Sessions, S. Abramovich, A. V. Turchyn, J. F. Adkins, Cenozoic record of δ34S in foraminiferal calcite implies an early Eocene shift to deep-ocean sulfide burial. *Nat. Geosci.* **11**, 761–765 (2018).

12. R. Tostevin, A. V. Turchyn, J. Farquhar, D. T. Johnston, D. L. Eldridge, J. K. B. Bishop, M. McIlvin, Multiple sulfur isotope constraints on the modern sulfur cycle. *Earth Planet. Sci. Lett.* **396**, 14–21 (2014).

13. G. E. Claypool, Ventilation of marine sediments indicated by depth profiles of pore water sulfate and δ34S, in *A Tribute to Isaac R. Kaplan*, R. J. Hill, J. Leventhal, Z. Aizenshtat, M. J. Baedereck, G. Claypool, R. Eganhouse, M. Goldhaber, K. Peters, Eds. (The Geochemical Society, 2004), pp. 59–65.

14. D. A. Fike, A. S. Bradley, C. V. Rose, Rethinking the ancient sulfur cycle. *Annu. Rev. Earth Planet. Sci.* **43**, 593–622 (2015).

15. X. Liu, D. Fike, A. Li, J. Dong, F. Xu, G. Zhuang, R. Rendle-Bühring, S. Wan, Pyrite sulfur isotopes constrained by sedimentation rates: Evidence from sediments on the East China Sea inner shelf since the late Pleistocene. *Chem. Geol.* **505**, 66–75 (2019).

16. V. Pasquier, P. Sansjofre, M. Rabineau, S. Revillon, J. Houghton, D. A. Fike, Pyrite sulfur isotopes reveal glacial-interglacial environmental changes. *Proc. Natl. Acad. Sci. U.S.A.* **114**, 5941–5945 (2017).

17. J. A. Richardson, C. Keating, A. Lepland, O. Hints, A. S. Bradley, D. A. Fike, Silurian records of carbon and sulfur cycling from Estonia: The importance of depositional environment on isotopic trends. *Earth Planet. Sci. Lett.* **512**, 71–82 (2019).

18. J. A. Richardson, M. Newville, A. Lanzirotti, S. M. Webb, C. V. Rose, J. G. Catalano, D. A. Fike, Depositional and diagenetic constraints on the abundance and spatial variability of carbonate-associated sulfate. *Chem. Geol.* **523**, 59–72 (2019).

19. C. Thomazo, A. Brayard, S. Elmeknassi, E. Vennin, N. Olivier, G. Caravaca, G. Escarguel, E. Fara, K. G. Bylund, J. F. Jenks, D. A. Stephen, B. Killingsworth, P. Sansjofre, P. Cartigny, Multiple sulfur

isotope signals associated with the late Smithian event and the Smithian/Spathian boundary. *Earth Sci. Rev.* **195**, 96–113 (2019).

20. B. B. Jørgensen, F. Beulig, M. Egger, C. Petro, C. Scholze, H. Røy, Organoclastic sulfate reduction in the sulfate-methane transition of marine sediments. *Geochim. Cosmochim. Acta* **254**, 231–245 (2019).

21. R. C. Aller, Sedimentary diagenesis, depositional environments, and benthic fluxes, in *Treatise on Geochemistry*, 2nd edition, H. Holland, K. K. Turekian, Eds. (Oxford: Elsevier, 2014),, pp. 293–334.

22. J. B. Ries, D. A. Fike, L. M. Pratt, T. W. Lyons, J. P. Grotzinger, Superheavy pyrite (δ34Spyr > δ34SCAS) in the terminal Proterozoic Nama Group, southern Namibia: A consequence of low seawater sulfate at the dawn of animal life. *Geology* **37**, 743–746 (2009).

23. R. C. Aller, V. Madrid, A. Chistoserdov, J. Y. Aller, C. Heilbrun, Unsteady diagenetic processes and sulfur biogeochemistry in tropical deltaic muds: Implications for oceanic isotope cycles and the sedimentary record. *Geochim. Cosmochim. Acta* **74**, 4671–4692 (2010).

24. M. Solan, E. R. Ward, E. L. White, E. E. Hibberd, C. Cassidy, J. M. Schuster, R. Hale, J. A. Godbold, Worldwide measurements of bioturbation intensity, ventilation rate, and the mixing depth of marine sediments. *Scientific Data* **6**, 58 (2019).

25. J. Adams, Contemporary uplift and erosion of the Southern Alps, New Zealand. *Geol. Soc. Am. Bull.* **91**, 1–114 (1980).

26. P. R. King, Tectonic reconstructions of New Zealand: 40 Ma to the present. *New Zeal. J. Geol. Geophys.* **43**, 611–638 (2000).

27. L. Carter, R. M. Carter, I. N. McCave, Evolution of the sedimentary system beneath the deep Pacific inflow off eastern New Zealand. *Mar. Geol.* **205**, 9–27 (2004).

28. C. S. Fulthorpe, R. M. Carter, Continental-shelf progradation by sediment-drift accretion. *Geol. Soc. Am. Bull.* **103**, 300–309 (1991).

29. H. Lu, C. S. Fulthorpe, Controls on sequence stratigraphy of a middle Miocene-Holocene, current-swept, passive margin: Offshore Canterbury Basin, New Zealand. *Geol. Soc. Am. Bull.* **116**, 1345–1366 (2004).

30. H. Lu, C. S. Fulthorpe, P. Mann, Three-dimensional architecture of shelf-building sediment drifts in the offshore Canterbury Basin New Zealand. *Mar. Geol.* **193**, 19–47 (2003).

31. K. Hoyanagi, S. Kawagata, S. Koto, T. Kamihashi, M. Ikehara, Data report: Pleistocene benthic foraminiferal oxygen and stable carbon isotopes and their application for age models, *Proc. IODP* **317** (2014).

32. X. Ding, Y. Wu, W. Li, 0.9 Ma oxygen isotope stratigraphy for a shallow-water sedimentary transect across three IODP 317 sites in the Canterbury Bight of the southwest Pacific Ocean. *Palaeogeogr. Palaeoclimatol. Palaeoecol.* **465**, 1–13 (2017).

33. H. Elderfield, P. Ferretti, M. Greaves, S. Crowhurst, I. N. McCave, D. Hodell, A. M. Piotrowski, Evolution of ocean temperature and ice volume through the mid-Pleistocene climate transition. *Science* **337**, 704–709 (2012).

34. L. E. Lisiecki, M. E. Raymo, A Pliocene-Pleistocene stack of 57 globally distributed benthic δ18O records. *Paleoceanography* **20**, PA1003 (2005).

35. R. M. Carter, I. N. McCave, C. Richter, L. Carter, 7. Site 1123 North Chatham Drift—A 20-Ma record of the Pacific Deep Western Boundary Current, *Proc. ODP Init. Rep.* **181**, 1–184 (1999).

36. C. S. Fulthorpe, K. Hoyanagi, P. Blum, J. Geldmacher, *Global and Local Controls on Continental Margin Stratigraphy: Canterbury Basin, Eastern South Island, New Zealand* (IODP Scientific Prospectus, 2009).

37. C. M. McHugh, C. S. Fulthorpe, K. Hoyanagi, P. Blum, G. S. Mountain, K. G. Miller, The sedimentary imprint of Pleistocene glacio-eustasy: Implications for global correlations of seismic sequences. *Geosphere* **14**, 265–285 (2017).

38. D. A. V. Stow, J.-C. Faugères, Contourites, turbidites and process interaction. *Sediment. Geol.* **115**, 1–384 (1998).

39. K. G. Miller, M. A. Kominz, J. V. Browning, J. D. Wright, G. S. Mountain, M. E. Katz, P. J. Sugarman, B. S. Cramer, N. Christie-Blick, S. F. Pekar, The Phanerozoic record of global sea-level change. *Science* **310**, 1293–1298 (2005).

40. J. C. Zachos, M. Pagani, L. Sloan, E. Thomas, K. Billups, Trends rhythms and aberrations in global climate 65 Ma to present. *Science* **292**, 686–693 (2001).

41. S. Arndt, B. B. Jørgensen, D. E. LaRowe, J. J. Middelburg, R. D. Pancost, P. Regnier, Quantifying the degradation of organic matter in marine sediments: A review and synthesis. *Earth Sci. Rev.* **123**, 53–86 (2013).

42. J. Middlelburg, A simple rate model for organic matter decomposition in marine sediments. *Geochim. Cosmochim. Acta* **53**, 1577–1581 (1989).

43. D. L. Eldridge, W. Guo, J. Farquhar, Theoretical estimates of equilibrium sulfur isotope effects in aqueous sulfur systems: Highlighting the role of isomers in the sulfite and sulfoxylate systems. *Geochim. Cosmochim. Acta* **195**, 171–200 (2016).

44. N. J. Shackleton, J. P. Kennett, Paleotemperature history of the Cenozoic and the initiation of Antartica glaciation: Oxygen and carbon analyses in DSDP sites 277, 279 and 281. *Init. Rep. DSDP* **29**, 743–755 (1975).

45. M.-X. Zhu, K.-K. Chen, G.-P. Yang, D.-J. Fan, T. Li, Sulfur and iron diagenesis in temperate unsteady sediments of the East China Sea inner shelf and a comparison with tropical mobile mud belts (MMBs). *J. Geophys. Res. Biogeo.* **121**, 2811–2828 (2016).

46. I. R. Hall, I. N. McCave, N. J. Shackleton, G. P. Weedon, S. E. Harris, Intensified deep Pacific inflow and ventilation in Pleistocene glacial times. *Nature* **412**, 809–812 (2001).

47. D. T. Rickard, Kinetics and mechanism of pyrite formation at low temperatures. *Am. J. Sci.* **275**, 636–652 (1975).

48. G. W. Luther III, Pyrite synthesis via polysulfide compounds. *Geochim. Cosmochim. Acta* **55**, 2839–2849 (1991).

49. D. T. Rickard, Kinetics of pyrite formation by the H2S oxidation of iron (II) monosulfide in aqueous solutions between 25 and 125°C: The rate equation. *Geochim. Cosmochim. Acta* **61**, 115–134 (1997).

50. J. Thiel, J. M. Byrne, A. Kappler, B. Schink, M. Pester, Pyrite formation from FeS and H2S is mediated through microbial redox activity. *Proc. Natl. Acad. Sci. U.S.A.* **116**, 6897–6902 (2019).

51. I. B. Butler, M. E. Böttcher, D. Rickard, A. Oldroyd, Sulfur isotope partitioning during experimental formation of pyrite via the polysulfide and hydrogen sulfide pathways: Implications for the interpretation of sedimentary and hydrothermal pyrite isotope records. *Earth Planet. Sci. Lett.* **228**, 495–509 (2004).

52. A. V. Turchyn, O. Sivan, D. P. Schrag, Oxygen isotopic composition of sulfate in deep sea pore fluid evidence for rapid sulfur cycling. *Geobiology* **4**, 191–201 (2006).

53. H. Fossing, B. B. Jørgensen, Isotope exchange reactions with radiolabeled sulfur compounds in anoxic seawater. *Biogeochemistry* **9**, 223–245 (1990).

54. H. Fossing, S. Thode-Andersen, B. B. Jørgensen, Sulfur isotope exchange between 35S-labeled inorganic sulfur compounds in anoxic marine sediments. *Mar. Chem.* **38**, 117–132 (1992).

55. S. E. Peters, J. M. Husson, Sediment cycling on continental and oceanic crust. *Geology* **45**, 323–326 (2017).

56. D. S. Jones, D. A. Fike, Dynamic sulfur and carbon cycling through the end-Ordovician extinction revealed by paired sulfate–pyrite δ34S. *Earth Planet. Sci. Lett.* **363**, 144–155 (2013).

57. C. V. Rose, W. W. Fischer, S. Finnegan, D. A. Fike, Records of carbon and sulfur cycling during the Silurian Ireviken Event in Gotland, Sweden. *Geochim. Cosmochim. Acta* **246**, 299–316 (2019).

58. J. Liu, A. Pellerin, G. Antler, S. Kasten, A. J. Findlay, I. Dohrmann, H. Røy, A. V. Turchyn, B. B. Jørgensen, Early diagenesis of iron and sulfur in Bornholm Basin sediments: The role of near-surface pyrite formation. *Geochim. Cosmochim. Acta* **284**, 43–60 (2020).

59. C. S. Fulthorpe, K. Hoyanagi, P. Blum, IODP Expedition 317: Exploring the record of sea-level change off New Zealand. *Sci. Drill.* **12**, 4–14 (2011).

60. L. Carter, I. N. McCave, The sedimentary regime beneath the deep western boundary current inflow to the southwest Pacific Ocean. *J. Sediment. Res.* **67**, 1005–1017 (1997).

61. R. M. Carter, L. Carter, I. N. McCave, Current controlled sediment deposition from the shelf to the deep ocean the Cenozoic evolution of circulation through the SW Pacific gateway. *Geol. Rundsch.* **85**, 438–451 (1996).

62. D. E. Canfield, R. Raiswell, J. T. Westrich, C. M. Reaves, R. A. Berner, The use of chromium reduction in the analysis of reduced inorganic sulfur in sediments and shales. *Chem. Geol.* **54**, 149–155 (1986).

63. S. W. Poulton, D. E. Canfield, Development of a sequential extraction procedure for iron: Implications for iron partitioning in continentally derived particulates. *Chem. Geol.* **214**, 209–221 (2005).

64. T. Goldberg, C. Archer, D. Vance, B. Thamdrup, A. McAnena, S. W. Poulton, Controls on Mo isotope fractionations in a Mn-rich anoxic marine sediment, Gullmar Fjord, Sweden. *Chem. Geol.* **296-297**, 73–82 (2012).

65. A. Matthews, I. Azrieli-Tal, A. Benkovitz, M. Bar-Matthews, D. Vance, S. W. Poulton, N. Teutsch, A. Almogi-Labin, C. Archer, Anoxic development of sapropel S1 in the Nile Fan inferred from redox sensitive proxies, Fe speciation, Fe and Mo isotopes. *Chem. Geol.* **475**, 24–39 (2017).

66. S. Henkel, S. Kasten, S. W. Poulton, M. Staubwasser, Determination of the stable iron isotopic composition of sequentially leached iron phases in marine sediments. *Chem. Geol.* **421**, 93–102 (2016).

67. L. E. Hepburn, I. B. Butler, A. Boyce, C. Schröder, The use of operationally-defined sequential Fe extraction methods for mineralogical applications: A cautionary tale from Mössbauer spectroscopy. *Chem. Geol.* **543**, 119584 (2020).

68. S. W. Poulton, M. D. Krom, R. Raiswell, A revised scheme for the reactivity of iron (oxyhydr)oxide minerals towards dissolved sulfide. *Geochim. Cosmochim. Acta* **68**, 3703–3715 (2004).

69. L. L. Stookey, Ferrozine-a new spectrophotometric reagent for iron. *Anal. Chem.* **42**, 779–781 (1970).

70. V. Pasquier, P. Sansjofre, O. Lebeau, C. Liorzou, M. Rabineau, Acid digestion on river influenced shelf sediment organic matter: Carbon and nitrogen contents and isotopic ratios. *Rapid Commun. Mass Spectrom.* **32**, 86–92 (2018).

71. M. E. Böttcher, B.-K. Khim, A. Suzuki, M. Gehre, U. G. Wortmann, H.-J. Brumsack, Microbial sulfate reduction in deep sediments of the Southwest Pacific (ODP leg 181, sites 1119–1125): Evidence from stable sulfur isotope fractionation and pore water modeling. *Mar. Geol.* **205**, 249–260 (2004).

72. N. Balci, W. C. Shanks, B. Mayer, K. W. Mandernack, Oxygen and sulfur isotope systematics of sulfate produced by bacterial and abiotic oxidation of pyrite. *Geochim. Cosmochim. Acta* **71**, 3796–3811 (2007).

73. L. Shawar, I. Halevy, W. Said-Ahmad, S. Feinstein, V. Boyko, A. Kamyshny, A. Amrani, Dynamics of pyrite formation and organic matter sulfurization in organic-rich carbonate sediments. *Geochim. Cosmochim. Acta* **241**, 219–239 (2018).

74. M. D. Simmons, Chapter 13 - Sequence stratigraphy and sea-level change, in *The Geologic Time Scale*, F. M. Gradstein, J. G. Ogg, M. D. Schmitz, G. M. Ogg, Eds. (Elsevier, 2012), pp. 239–267.

75. I. W. Croudace, R. G. Rothwell, *Micro-XRF Studies of Sediment Cores* (Developments in Paleoenvironmental Research, Springer, 2015), pp. XXIX–656.

76. Z. Lin, X. Sun, H. Strauss, Y. Lu, M. E. Böttcher, B. M. A. Teichert, J. Gong, L. Xu, J. Liang, H. Lu, J. Peckmann, Multiple sulfur isotopic evidence for the origin of elemental sulfur in an iron-dominated gas hydrate-bearing sedimentary environment. *Mar. Geol.* **403**, 271–284 (2018).

77. P. Meister, B. Brunner, A. Picard, M. E. Bottcher, B. B. Jorgensen, Sulphur and carbon isotopes as tracers of past sub-seafloor microbial activity. *Sci. Rep.* **9**, 604 (2019).

78. B. U. Haq, S. R. Schutter, A chronology of Paleozoic sea-level changes. *Science* **322**, 64–68 (2008).

79. Y. Xiao, K. Wu, L. Tian, M. J. Benton, Y. Du, H. Yang, J. Tong, Framboidal pyrite evidence for persistent low oxygen levels in shallow-marine facies of the Nanpanjiang Basin during the Permian-Triassic transition. *Palaeogeogr. Palaeoclimatol. Palaeoecol.* **511**, 243–255 (2018).

80. T. Algeo, Y. Shen, T. Zhang, T. Lyons, S. Bates, H. Rowe, T. K. T. Nguyen, Association of ^{34}S-depleted pyrite layers with negative carbonate δ^{13}C excursions at the Permian-Triassic boundary: Evidence for upwelling of sulfidic deep-ocean water masses. *Geochem. Geophys. Geosyst.* **9**, Q04025 (2008).

81. P. Gorjan, K. Kaiho, T. Kakegawa, S. Niitsuma, Z. Q. Chen, Y. Kajiwara, A. Nicora, Paleoredox, biotic and sulfur-isotopic changes associated with the end-Permian mass extinction in the western Tethys. *Chem. Geol.* **244**, 483–492 (2007).

82. T. Algeo, C. M. Henderson, B. Ellwood, H. Rowe, E. Elswick, S. Bates, T. Lyons, J. C. Hower, C. Smith, B. Maynard, L. E. Hays, R. E. Summons, J. Fulton, K. H. Freeman, Evidence for a diachronous Late Permian marine crisis from the Canadian Arctic region. *Geol. Soc. Am. Bull.* **124**, 1424–1448 (2012).

83. S. E. Grasby, B. Beauchamp, Latest Permian to Early Triassic basin-to-shelf anoxia in the Sverdrup Basin, Arctic Canada. *Chem. Geol.* **264**, 232–246 (2009).

84. D. P. G. Bond, P. B. Wignall, The role of sea-level change and marine anoxia in the Frasnian–Famennian (Late Devonian) mass extinction. *Palaeogeogr. Palaeoclimatol. Palaeoecol.* **263**, 107–118 (2008).

85. M. M. Joachimski, C. Ostertag-Henning, R. D. Pancost, H. Strauss, K. H. Freeman, R. Littke, J. S. Sinninghe Damsté, G. Racki, Water column anoxia, enhanced productivity and concomitant changes in d13C and d34S across the Frasnian-Famennian boundary (Kowala–Holy Cross Mountains/Poland). *Chem. Geol.* **175**, 109–131 (2001).

86. M. S. Sim, S. Ono, M. T. Hurtgen, Sulfur isotope evidence for low and fluctuating sulfate levels in the Late Devonian ocean and the potential link with the mass extinction event. *Earth Planet. Sci. Lett.* **419**, 52–62 (2015).

87. H. H. J. Geldsetzer, W. D. Goodfellow, D. J. McLaren, M. J. Orchard, Sulfur-isotope anomaly associated with the Frasnian-Famennian extiction, Medecine lake, Alberta, Canada. *Geology* **15**, 393–396 (1987).

88. D. Chen, J. Wang, G. Racki, H. Li, C. Wang, X. Ma, M. T. Whalen, Large sulphur isotopic perturbations and oceanic changes during the Frasnian-Famennian transition of the Late Devonian. *J. Geol. Soc. London* **170**, 465–476 (2013).

89. M. E. Johnson, Relationship of Silurian sea-level fluctuations to oceanic episodes and events. *Gff* **128**, 115–121 (2006).

90. E. Kiipli, T. Kiipli, Hirnantian sea-level changes in the Baltoscandian Basin, a review. *Palaeogeogr. Palaeoclimatol. Palaeoecol.* **540**, 109524 (2020).

91. P. Gorjan, K. Kaiho, D. A. Fike, C. Xu, Carbon- and sulfur-isotope geochemistry of the Hirnantian (Late Ordovician) Wangjiawan (Riverside) section, South China: Global correlation and environmental event interpretation. *Palaeogeogr. Palaeoclimatol. Palaeoecol.* **337-338**, 14–22 (2012).

92. S. A. Young, E. Benayoun, N. P. Kozik, O. Hints, T. Martma, S. M. Bergström, J. D. Owens, Marine redox variability from Baltica during extinction events in the latest Ordovician–early Silurian. *Palaeogeogr. Palaeoclimatol. Palaeoecol.* **554** 109792 (2020).

93. C. Zou, Z. Qiu, H. Wei, D. Dong, B. Lu, Euxinia caused the Late Ordovician extinction: Evidence from pyrite morphology and pyritic sulfur isotopic composition in the Yangtze area, South China. *Palaeogeogr. Palaeoclimatol. Palaeoecol.* **511**, 1–11 (2018).

94. D. Yan, D. Chen, Q. Wang, J. Wang, Z. Wang, Carbon and sulfur isotopic anomalies across the Ordovician-Silurian boundary on the Yangtze Platform, South China. *Palaeogeogr. Palaeoclimatol. Palaeoecol.* **274**, 32–39 (2009).

95. M. R. Saltzman, R. L. Ripperdan, M. D. Brasier, K. C. Lohmann, R. A. Robison, W. T. Chang, S. Peng, E. K. Ergaliev, B. Runnegar, A global carbon isotope excursion (SPICE) during the Late Cambrian: Relation to trilobite extinctions, organic-matter burial and sea level. *Palaeogeogr. Palaeoclimatol. Palaeoecol.* **162**, 211–223 (2000).

96. B. C. Gill, T. W. Lyons, H. C. Jenkyns, A global perturbation to the sulfur cycle during the Toarcian Oceanic Anoxic Event. *Earth Planet. Sci. Lett.* **312**, 484–496 (2011).

97. M. T. Hurtgen, S. B. Pruss, A. H. Knoll, Evaluating the relationship between the carbon and sulfur cycles in the later Cambrian ocean: An example from the Port au Port Group, western Newfoundland, Canada. *Earth Planet. Sci. Lett.* **281**, 288–297 (2009).

98. R. M. Mitchum, J. C. Van Wagoner, High-frequency sequences and their stacking patterns: Sequence-stratigraphic evidence of high-frequency eustatic cycles. *Sediment. Geol.* **70**, 131–160 (1991).